

# The enigma of the oldest ‘nova’: the central star and nebula of CK Vul

M. Hajduk,<sup>1</sup> Albert A. Zijlstra,<sup>2</sup> P.A.M. van Hoof,<sup>3</sup> J. A. Lopez<sup>4</sup>, J.E. Drew<sup>5</sup>,  
 A. Evans,<sup>6</sup> S.P.S. Eyres,<sup>7</sup> K. Gesicki,<sup>1</sup> R. Greimel,<sup>8</sup> F. Kerber,<sup>9</sup>  
 S. Kimeswenger<sup>10</sup> and M.G. Richer<sup>4</sup>

<sup>1</sup> *Centrum Astronomii UMK, ul. Gagarina 11, PL-87-100 Torun, Poland*

<sup>2</sup> *University of Manchester, School of Physics & Astronomy, P.O. Box 88, Manchester M60 1QD, UK*

<sup>3</sup> *Royal Observatory of Belgium, Ringlaan 3, Brussels, Belgium*

<sup>4</sup> *Instituto de Astronomia, Universidad Nacional Autonoma de Mexico, Apdo. Postal 877, 22800 Ensenada, BC, Mexico*

<sup>5</sup> *Imperial College of Science, Technology and Medicine, Blackett Laboratory, Prince Consort Road, London, SW7 2BW, UK*

<sup>6</sup> *Department of Physics, School of Chemistry and Physics, Keele University, Staffordshire ST5 5BG, UK*

<sup>7</sup> *Centre for Astrophysics, University of Central Lancashire, Preston PR1 2HE, UK*

<sup>8</sup> *Isaac Newton Group of Telescopes, Apartado de correos 321, E-38700 Santa Cruz de La Palma, Tenerife, Spain*

<sup>9</sup> *European Southern Observatory, Karl-Schwarzschild-Strasse 2, D-85748 Garching, Germany*

<sup>10</sup> *Institut für Astro- und Teilchenphysik, Universität Innsbruck, Technikerstr. 25, 6020 Innsbruck, Austria*

Accepted Received; in original form

## ABSTRACT

CK Vul is classified as, amongst others, the slowest known nova, a hibernating nova, or a very late thermal pulse object. Following its eruption in AD 1670, the star remained visible for 2 years. A 15-arcsec nebula was discovered in the 1980’s, but the star itself has not been detected since the eruption. We here present radio images which reveal an 0.1-arcsec radio source with a flux of 1.5 mJy at 5 GHz. Deep H $\alpha$  images show a bipolar nebula with a longest extension of 70 arcsec, with the previously known compact nebula at its waist. The emission-line ratios show that the gas is shock-ionized, at velocities  $> 100 \text{ km s}^{-1}$ . Dust emission yields an envelope mass of  $\sim 5 \times 10^{-2} M_{\odot}$ . Echelle spectra indicate outflow velocities up to  $360 \text{ km s}^{-1}$ . From a comparison of images obtained in 1991 and 2004 we find evidence for expansion of the nebula, consistent with an origin in the 1670 explosion; the measured expansion is centred on the radio source. No optical or infrared counterpart is found at the position of the radio source. The radio emission is interpreted as thermal free-free emission from gas with  $T_e \sim 10^4 \text{ K}$ . The radio source may be due to a remnant circumbinary disk, similar to those seen in some binary post-AGB stars. We discuss possible classifications of this unique outburst, including that of a sub-Chandrasekhar mass supernova, a nova eruption on a cool, low-mass white dwarf, or a thermal pulse induced by accretion from a circumbinary disk.

**Key words:** Stars: CK Vul Stars: mass loss; Stars: evolution; Stars: binary; Stars: Post-AGB; Planetary nebulae

## 1 INTRODUCTION

The enigmatic CK Vul (Shara & Moffat 1982) is currently the oldest catalogued nova variable.<sup>1</sup> Its classification remains controversial. The star was first observed by Père Dom Anthelme and was discovered independently by

Hevelius in June/July 1670. The observed eruption lasted for two years, during 1670-1672. It was discovered at 3rd magnitude, and faded over 100 days to below visual limits (magnitude 6). The following year it was recovered during rebrightening, reaching magnitude 2.6, 300 days after the first maximum. It again faded on the same time scale of 100 days to below observational limits. It showed a faint tertiary maximum 600 days after the first peak, at magnitude 5.5 (Shara et al. 1985). The star has not been recovered since. Its light curve is unlike any catalogued novae, raising doubts

<sup>1</sup> Of the eruptive variables, it is predated only by the well-known Galactic supernovae and by the LBV eruptions of P Cyg in 1600 and 1655

on its status. Interpretations include a hibernating nova, or a helium flash on a new white dwarf.

The historic observations provided coordinates for CK Vul accurate to within a few arcminutes. Based on the old charts, Shara & Moffat (1982) were successful in searching for the remnant. They discovered several nebulosities on their  $H\alpha + [N II]$  image, the spectra of which present reddened emissions of  $[N II]$ ,  $H II$ ,  $[O II]$  and  $[S II]$ . On their spectra, the flux of  $[N II] \lambda 6584\text{\AA}$  is three times more intense than the  $H\alpha$  line, indicating an evolved, and perhaps hydrogen deficient chemical composition. No obvious exciting star was found in the field of CK Vul. A central star candidate was suggested by Shara et al. (1985), but shown to be misidentified as such by Naylor et al. (1992); the latter authors were unable to identify, among the stars visible on their R image, an alternative central star candidate which could be responsible for the ionization of the observed nebulosity.

The lack of bright candidates for the central star would constrain the possible companion of the white dwarf in cataclysmic systems, assuming that CK Vul is an ordinary nova. However, the list of features uncommon for classical novae is extensive. The light curve during the outburst of Nova Vul 1670 is unprecedented, showing variations which resemble a set of declines and subsequent recoveries. The rebrightenings may indicate constant intrinsic brightness with intermittent dust formation, or a light echo. In the first instance, the object remained at high luminosity for over a year, with the fading(s) caused by intermittent extinction. In the second case, a dense medium needs to be present within a parsec of the source. The properties of the shell are quite unusual: a low outflow velocity of the ejected material, low density and high ionized mass (although the distance is very uncertain). Shara et al. (1985) discuss (and reject) some alternative hypotheses concerning the nature of CK Vul. Harrison (1996) suggests that CK Vul may be a Very Late Thermal Pulse event (VLTP) rather than a nova: this is based on similarities of the light curve to those seen in V605 Aql and V4334 Sgr (Sakurai's Object) (Hajduk et al. 2005). Evans et al. (2002) have added more arguments for this reborn scenario for CK Vul. If the VLTP scenario for CK Vul is correct, it would be only the third object observed during a VLTP. Kato (2003) suggested CK Vul to be a stellar merger. However, none of the presented scenarios is fully convincing: the observational data are limited, but the object seems to be unique.

In order to test the VLTP hypothesis we searched for evidence of ionized material, since these stars reach high temperatures soon after the eruption and ionize a compact shell. In contrast, radio emission from classical novae fades within a few years after the eruption. To this end we conducted radio observations and also obtained deep images, to search for the ejecta, and for evidence of a fossil planetary nebula.

## 2 OBSERVATIONS

### 2.1 Radio emission

The first radio observations of CK Vul were carried out with the VLA array on the 4<sup>th</sup> of April 2005. The VLA was in the so-called 'B' configuration, with a largest baseline of about

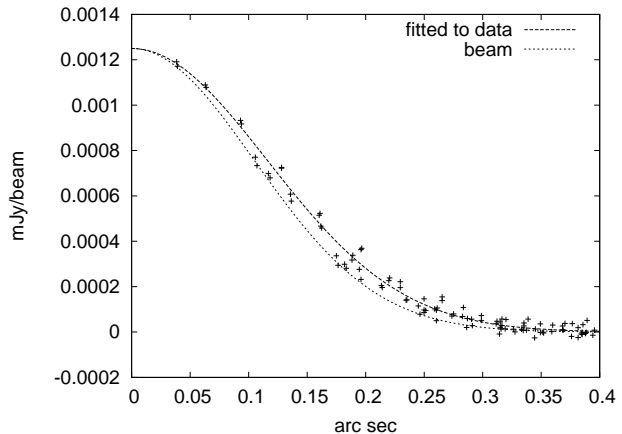


**Figure 1.** The profile of the radio source, based on the higher resolution 8 GHz 2006 observations.

10 km. The observations were done at a frequency of 5 GHz. CK Vul was observed for approximately 2 hours, divided into  $\sim 14$ -min scans, interspersed with observations of the phase calibrator (1922+155). A second set of observations was obtained on April 9, 2006, with the VLA in the 'A' configuration. After each  $\sim 10$  min scan of CK Vul, at 5 GHz and 8 GHz, alternately, the phase calibrator 1922+155 was observed.

1331+305 was used as the primary flux calibrator for both the 2005 and 2006 observations. Observational parameters are summarized in Table 1.

The data were reduced using standard procedures implemented in the AIPS package, by Fourier transforming the visibility data followed by the removal of the dirty beam pattern. The data were convolved with a synthesized gaussian point spread function (beam) of the same FWHM as the dirty beam: the beam sizes are listed in Table 1. Low spatial resolution images were also created, in order to search for confusing sources: only a few such confusing sources were found at 5 GHz and 8 GHz. Both uniformly and naturally weighted images were made, using the CLEAN algorithm. The RMS noise on the maps of CK Vul followed closely the theoretical thermal noise.

Our 2005 observation reveals radio emission of  $1.46 \pm 0.05$  mJy (where the uncertainty is taken as the  $3\text{-}\sigma$  noise on the map). The emission is consistent with a point source: the upper limit of the diameter, deconvolved from the beam, is 0.5 arcsec. But the higher resolution 2006 observations find the object to be resolved. The profile of the source, and that of the beam are shown in Fig 1. The FWHM of the beam is  $0.26 \times 0.23$  arcsec, the convolved source  $0.29 \times 0.26$  arcsec, and the deconvolved FWHM (gaussian fit) is  $0.12 \pm 0.01 \times 0.11 \pm 0.01$  arcsec. The fitting rules out a point source.

The fluxes are listed in Table 1: they were measured both from gaussian fitting and from summing. The slight difference between the two epochs may be due to calibration uncertainties or intrinsic variability. The peak intensity of the 8 GHz emission (natural weighting) is  $1.25 \pm 0.02$  mJy/beam, lower than the integrated flux. This also confirms that the source is resolved. The source is not circularly polarized, but due to the faintness of the source the detection limit for polarization is only about 20 per cent.

**Table 1.** Observational parameters for the VLA observations (naturally weighted images). The radio source is at position (J2000)  $19^{\text{h}} 47^{\text{m}} 38.074^{\text{s}} + 27^{\circ} 18' 45.16''$ 

Date	Freq.	$t_{\text{int}}$	Beam FWHM	pa deg	flux mJy	$\sigma$ mJy/beam	1922+155 flux mJy	1331+305 flux Jy
4 Apr 2005	5 GHz	2 h	$1.52'' \times 1.36''$	-54	1.46	0.016	682	4.66
9 Apr 2006	5 GHz	1 h	$0.46'' \times 0.38''$	+5	1.27	0.030	660	4.66
9 Apr 2006	8 GHz	1 h	$0.26'' \times 0.23''$	-1	1.53	0.023	651	7.34

## 2.2 H $\alpha$ observations

### 2.2.1 INT

The field of CK Vul was observed on two different occasions at the Isaac Newton Telescope (INT), located on La Palma. The first observations were carried out during a service night on Aug 4, 2004, and the second were obtained as part of the IPHAS survey, on July 12, 2005. IPHAS is a CCD H $\alpha$  imaging survey of the Northern Galactic plane (Drew et al. 2005). This survey uses 120-sec exposures through the H $\alpha$  filter, 30 sec through the Sloan  $r'$  and 10 sec through Sloan  $i'$  (every sky position is covered twice). The deeper service observations used three 600-sec H $\alpha$  exposures, supplemented by three 90-sec exposures with the Sloan  $r'$  filter. All observations used the wide field camera, which has a 30 arcmin field of view, mapped onto a mosaic of 4 CCDs. The pixel size is 0.3 arcsec.

The observations were taken using the IPHAS observing procedures and were reduced using the IPHAS pipeline: the procedure includes bias subtraction, flat-fielding, non-linearity correction and astrometric fit. The emission associated with CK Vul was centred on one of the four CCDs. The pipeline also obtains photometry of all point sources in the field, stored in a catalogue. The 2004 observations were taken under non-photometric conditions, with intermittent high cloud.

The  $r'$  filter is used for the continuum subtraction, but it should be noted that its broad coverage (5500–7000Å) also covers H $\alpha$ . The H $\alpha$  filter has a width of 95Å, and includes the [N II] lines. An emission line image was obtained from the difference of the H $\alpha$  and  $r'$  images.

The H $\alpha$  and  $r'$  observations have different values for the image quality. A direct subtraction of the  $r'$  image therefore leaves significant stellar residuals—we note that the field is very crowded. Both positive and negative residuals are also caused by the fact that stars show variable  $r'$ –H $\alpha$  colours due to the stellar H $\alpha$  absorption, and by TiO bands for M stars. This can affect the  $r'$ –H $\alpha$  colour by as much as a magnitude. To circumvent these problems, continuum subtraction was done in a different way. We used the DAOPHOT program to obtain a list of stellar positions for the  $r'$  image. This list was subsequently used to find the counterparts of these sources in the H $\alpha$  image. A point-spread function fitting was done to obtain the magnitude (in H $\alpha$ ), and to subtract these stellar sources. The same fitting and subtraction procedure was also carried out in the  $r'$  image. Finally, the residual  $r'$ -band image was subtracted from the residual H $\alpha$  image. This procedure greatly reduces the stellar residuals but may subtract true H $\alpha$  emission stars. We checked for

the presence of such stars in the area surrounding CK Vul but did not find any.

The astrometry of the image was re-calibrated using the positions of the stars in the Second US Naval Observatory CCD Astrograph Catalog (UCAC2 Zacharias et al. 2004). The accuracy of the astrometry, based on the RMS of the fit, is 0.1 arcsec.

Below we refer to the final image as 'the H $\alpha$  image' (adopting the name of the filter). However, the reader should be aware that the [N II] lines may contribute or even dominate the line emission within the filter pass band.

### 2.2.2 WHT

H $\alpha$  images have previously been presented by Naylor et al. (1992). The original data were kindly provided to us and re-reduced using IRAF. The observations were carried out at the William Herschel Telescope, on La Palma, on August 10, 1991. They made use of a small CCD at the auxiliary Cassegrain port; the scale is 0.1 arcsec/pixel. The observations in H $\alpha$  were de-biased and flat-field corrected. The image was calibrated with respect to the positions of the stars on the INT image: the RMS of the relative fit is 0.05 arcsec.

## 2.3 Long-slit spectrometry

The long-slit observations were obtained with the Manchester echelle spectrometer (MES: Meaburn et al. 2003) combined with the f/7.9 focus of the 2.1 m San Pedro Mártir, UNAM telescope, on 2006 July 12. This echelle spectrometer has no cross-disperser. For the present observations a filter of 90Å bandwidth was used to isolate the 87<sup>th</sup> order containing the H $\alpha$  and [N II] emission lines. A 1024  $\times$  1024 SITE CCD with 24 $\mu$ m pixels was used. Seeing conditions were variable, with a mean of 2 arcsec during the observations.

Four slit positions across CK Vul were obtained. The first two positions employed an on-chip binning factor 2  $\times$  2 and a slit width of 150 $\mu$ m, equivalent to 11 km s<sup>-1</sup> and 0.6 arcsec increments along the slit. However due to the faintness of the emission and the relatively poor seeing, the third and fourth positions were obtained with a 4  $\times$  4 binning and a 300 $\mu$ m wide slit corresponding to 20 km s<sup>-1</sup> resolution and 1.2 arcsec increments along the slit for better sensitivity. The slit orientations of the latter are shown in Fig. 7 and the spectra in Fig. 8. The slits were oriented in all cases N–S and the integration times were 1800 seconds. The spectra were reduced and calibrated in wavelength against a Th–Ar lamp using standard procedures.

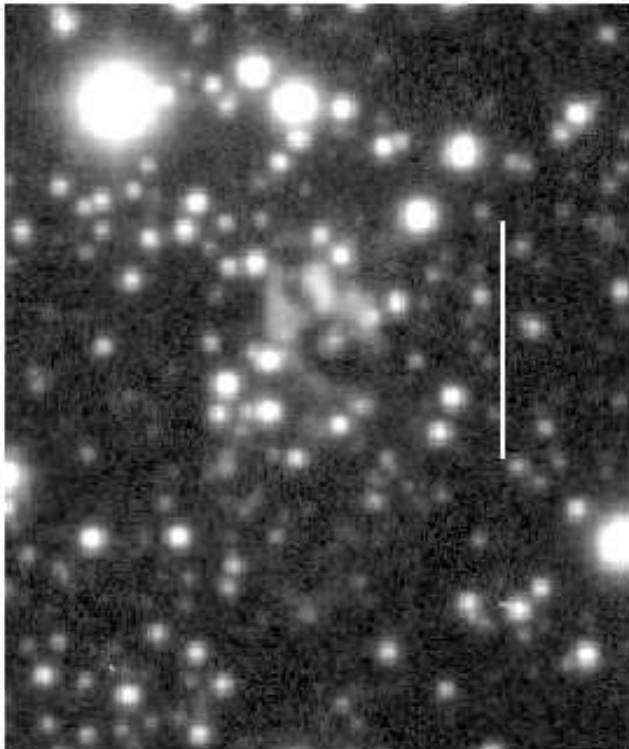


**Figure 2.** The INT  $H\alpha$  image of CK Vul, before continuum subtraction. A logarithmic intensity scale is used to bring out the faint emission. The vertical bar is 30 arcsec in length; North is at the top and East is left.

## 2.4 Other data

An earlier radio continuum observation of CK Vul at 20 cm was performed by Bode et al. (1987), on January 28, 1984. They found an upper limit of 1.52 mJy, with a spatial resolution of 14 arcsec. Due to the low resolution, this limit includes both the compact source and the extended nebulosity.

Proposed R-band and JHK counterparts are summarised in Evans et al. (2002). We consider these to be uncertain, referring to unrelated (field) stars. 2MASS finds all these to have the colours of normal stars. Observations in other wavelength regimes include flux measurements at 850 and 450  $\mu\text{m}$  and flux densities derived from re-analysis of the IRAS data (Evans et al. 2002). Upper limits were found for MSX (8.3  $\mu\text{m}$ ) and IRAS 100  $\mu\text{m}$ .

GLIMPSE/Spitzer images of the field confirm that all 2MASS sources show stellar Rayleigh-Jeans colours. This includes the star inside the cavity south of the radio source, which was studied by Harrison (1996).

## 3 RESULTS OF THE OBSERVATIONS

### 3.1 Optical lobes

The  $H\alpha$  image, derived from the Aug. 2004 (long) integrations, is shown in Fig. 2. It shows the dense star field, and the compact structure first found by Shara et al. (1985). The nebulosity appears as a partial ring, extending 15-arcsec across E-W. The star at the centre of the ring, originally

suspected to be CK Vul, is now thought to be a field star. Faint nebular emission is lost in the dense star field.

The corresponding continuum-subtracted optical image is presented in Fig. 3. The image shows that the previously known nebulosity is located at the waist of a much larger, bipolar structure. The bipolar lobes are edge-brightened: the filled emission is just visible in the northern lobe but is below the detection limit in the southern lobe. A number of small condensations are visible, two of which delineate the tips of the lobes. A bright condensation is seen on the SE lobe. The angular distance between the tips of the lobes is 70 arcsec. The filter transmission includes both  $H\alpha$  and  $[\text{N II}]$ , and either line may contribute in different areas of the structures.

The central region is shown in more detail in Fig. 3B. A funnel-like structure is seen, with one side much brighter than the other. (But whether the structure is in fact a cavity is not known.) Four other knots are visible: each of these components are numbered on the image as in Shara et al. (1985). An arc connects knots 2 and 4, but it is not part of a closed ring. The three-dimensional structure cannot easily be deduced from the image. In addition to the numbering of Shara et al. (1985), we number (6) the central diffuse source and (7) the more diffuse emission between knots 4 and 5.

We note that a stellar source on the western ring was subtracted in the continuum removal process. This left the blank residual below knot 3. Some compact  $H\alpha$  emission was likely subtracted in this process, as suggested by the residuals. This problem occurs when a star is much brighter than coincident  $H\alpha$  emission, but does not affect other locations within the nebulosity. Fig. 4A shows the inner region of  $r'$ -band INT image, where this star is visible to the West of the radio source.

### 3.2 Radio source

The radio emission is shown in Fig. 4A superposed on the INT  $r'$ -band image. The brightest emission-line regions are faintly visible in the  $r'$ -band, because the wavelengths of the emission lines fall within the filter transmission curve. The radio source is located between knots 1 and 6 (Fig. 3). Three stars located in the region below the funnel could be candidates for the central star, but they do not coincide with the compact radio source. The radio source also does not coincide with any of the  $H\alpha$ + $[\text{N II}]$  bright knots.

An accidental superposition of a background radio source is improbable, due to the excellent coincidence of the position of the radio emission with the nebula. Moreover, only one other source with comparable flux to the one referred to CK Vul was found in the full primary beam field (FWHM) of 9.0 arcmin.

The radio source is close to the brightest part of the elongated knot '1'. Fig. 4B shows the WHT image, which has better spatial resolution. A faint elongation or separate source is indicated just below knot '1'; on the INT image this merges with the knot because of the worse seeing. The faint elongation is within 0.5 arcsec of the radio source (right-most plus sign in Fig. 4B). It has a very faint  $r'$ -band counterpart, confirming it is an emission line region. To classify this extension as a separate source would require either higher angular resolution, or kinematic data. Given the extent of the emission line regions around the radio source, the likelihood

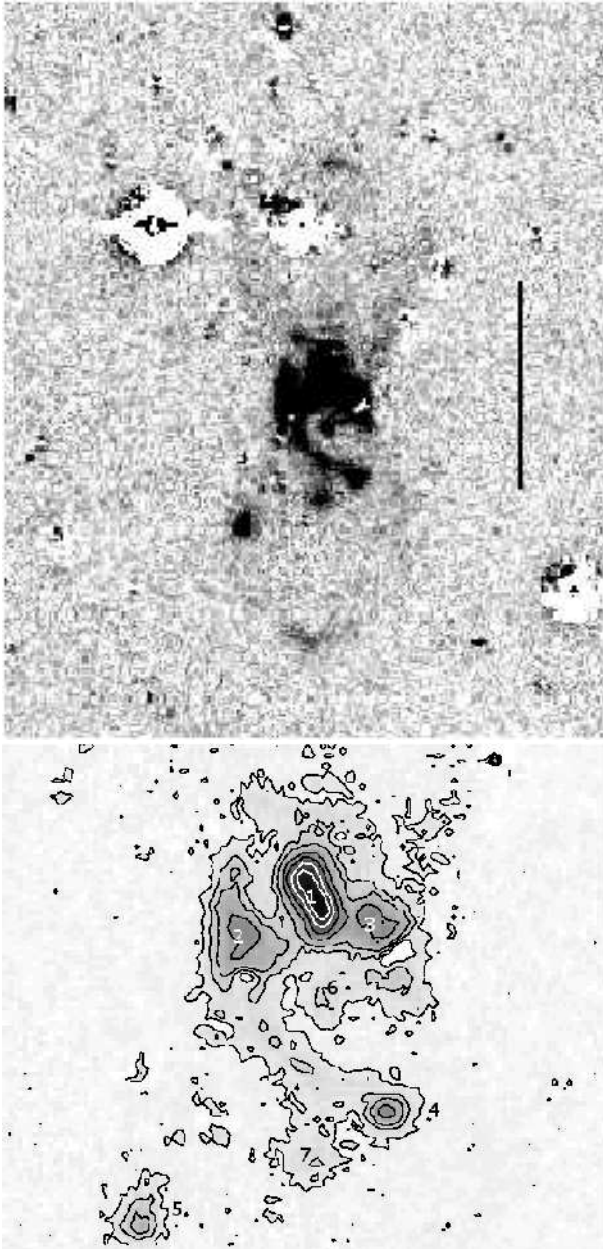


**Figure 3.** The continuum-subtracted INT  $H\alpha$  image of CK Vul. North is top, east is left. A (Top): Image encompassing all detected line emission. The contrast is set to bring out the faint bipolar lobes. The vertical bar is 30 arcsec in length. B (Bottom): The central region, corresponding to the emission detected by Shara et al. (1985). The linear contours and the grey scale refer to the same image. The peaks on either side of the apparent ‘funnel’ are 5 arcsec apart. The numbers 1 to 5 correspond to the knots detected by Shara et al. (1985). Numbers 6 & 7 have been added in this paper; see text for discussion.

of a chance superposition is rather high. However, it is our only –but speculative– candidate for an optical counterpart.

The radio source is situated in a cavity close to the brightest part of the nebulosity. Nebulosity located further from the radio source shows a tendency of decreasing brightness with distance from the radio source. This indicates that the radio source is associated with the current energy source

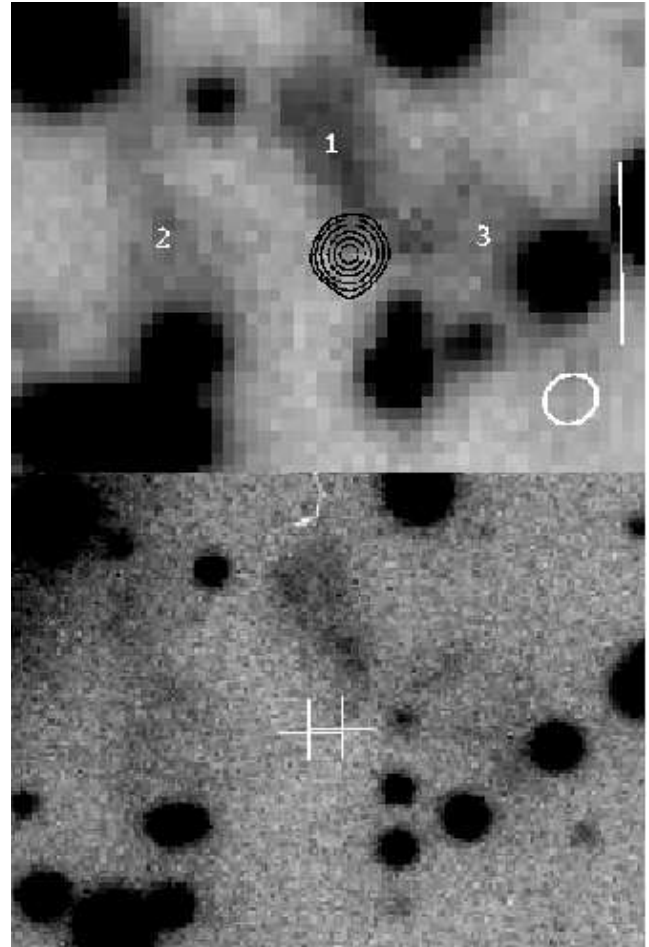


**Figure 4.** The radio source superposed on the optical images. North is top, east is left. The position of the radio source is  $19^{\text{h}} 47^{\text{m}} 38.074^{\text{s}} + 27^{\circ} 18' 45.16''$ . The knots are indicated by their numbers. A (top): superposed on the  $r'$ -band INT image. The image is 21.5 arcsec across horizontally. Radio contours are at 0.075, 0.15, 0.3, 0.6, 0.9, 1.2 mJy/beam, from the 2005 VLA observations (natural weighting). The oval indicates the size of the beam; the black bar is 5 arcsec long. B (bottom): superposed on the WHT  $H\alpha$  image. The right-most plus sign indicates the position of the radio source. The left-most plus sign gives the geometric centre of the bipolar lobes.

of the nebula, and reveals the position, if not the identification, of the central object.

The radio source is to a very good (1-arcsec) accuracy located at the centre of symmetry of the tips of the bipolar nebula. This point is indicated by the left-most plus sign in Fig. 4B. This also supports the identification of the radio source as the central object.

The INT data show that at the position of the radio source, there is no optical counterpart down to a conservative limit of  $r' > 23$ . The i-band IPHAS image is less deep, and gives a limit of  $i' > 20$ .

### 3.3 Expansion

The WHT image compared to the INT image allows us to search for temporal variations in the nebula. The WHT data were taken in 1991 and the INT data in 2004. The 13-year

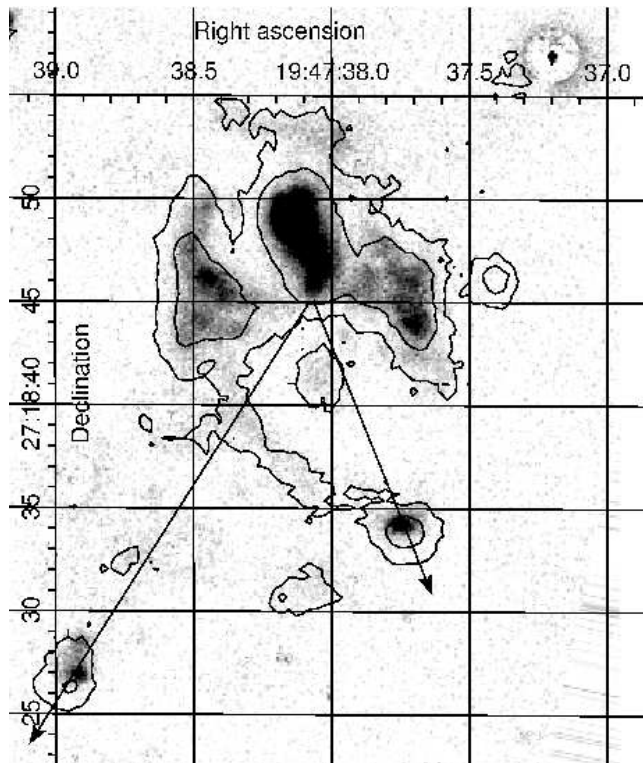


**Figure 5.** The WHT H $\alpha$  from 1991 (grey scale) together with the 2004 INT H $\alpha$  image (contours at 3 and 10  $\sigma$ ). Two compact components show significant proper motion. The arrows link the radio sources to these components: the direction is consistent with the observed proper motion.

separation represents 4 per cent of the elapsed time since the AD 1670 eruption.

In Fig. 5, the grey scale shows the WHT image, and the INT H $\alpha$  (including continuum) image is overlaid as contours. The WHT image does not cover the full region of the nebula (which was not known at the time). The images are aligned on the stellar positions. The relative (rms) accuracy is 0.05 arcsec.

Several emission-line nebulosities have changed position, in particular knots 4 and 5. (The object to the West of knot 3 has moved north: this is interpreted as a high proper motion star.) The change in position is away from the central radio source, as indicated by the arrows in Fig. 5. The positions of knots 4 and 5 are given in Table 2. The indicated relative motion from 1991 to 2004 is  $(\mu_\alpha, \mu_\delta) = (-0.16, -0.46)$  arcsec, and  $(\mu_\alpha, \mu_\delta) = (0.36, -0.67)$  arcsec, for knot 4 and 5, respectively.

The original positions of the two components are obtained by extrapolation back to 1670. The extrapolated position of knot 4 is coincident with the position of the radio source, assumed to represent the central star. The agreement is worse for knot 5, possibly due to its extended, irregular structure, which is better resolved in the WHT image than in the INT image (Table 2). Residual image distortions may also be present in the WHT images.

The observed motion of these two components, located outside the inner region of the nebula, implies that the observed lobes are indeed the remnants of the 1670 event. It

**Table 2.** Centroid positions (J2000) of the two components indicated in Fig. 5. The accuracy of the determination of centroids is typically about 0.02 arcsec, but for the component 5 at 2004 is a few times worse.

Component		1991 position	2004 position
4	$\alpha$	19 <sup>h</sup> 47 <sup>m</sup> 37.753 <sup>s</sup>	19 <sup>h</sup> 47 <sup>m</sup> 37.741 <sup>s</sup>
	$\delta$	+27° 18' 34.31''	+27° 18' 33.85''
5	$\alpha$	19 <sup>h</sup> 47 <sup>m</sup> 38.931 <sup>s</sup>	19 <sup>h</sup> 47 <sup>m</sup> 38.958 <sup>s</sup>
	$\delta$	+27° 18' 27.18''	+27° 18' 26.51''

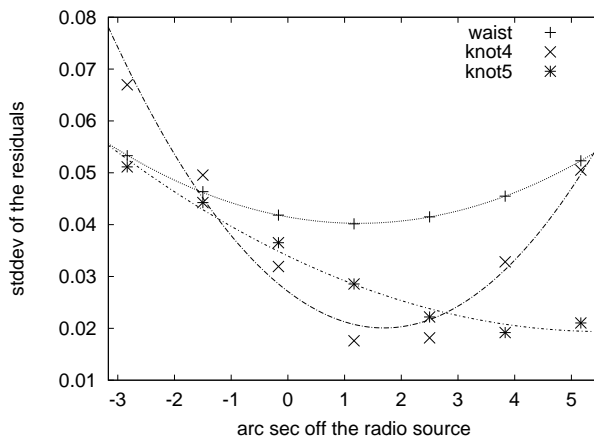


**Figure 6.** The residuals of the scaled IPHAS image and the WHT H $\alpha$  images, versus the position of the assumed expansion centre. The position of radio source is at 0.

also confirms our interpretation of the radio source as the eruptive object.

To improve the sensitivity to expansion, we subtracted the IPHAS image from the WHT observations. The subtracted image showed residuals at the position of the two outer, moving knots, the central brightest nebulosities, the faint arc and other nebular structures, present on the H $\alpha$  image. Applying a constant scaling factor prior to the subtraction, to reduce the image scale of the IPHAS image, greatly reduced these residuals.

Figure 6 shows the residuals of the two knots, and the brightest part of the inner nebula, for different positions of the centre of the expansion. The best fit was obtained for the assumed expansion centre lying within 2 arcsec of the radio emission. The constant scaling factor assumes that the material seen in the field of CK Vul is coming from the 1670 eruption event and is flowing ballistically.

Unfortunately, the tips of the lobes of the outer nebula are outside of the WHT frame. However, the tip of the southern lobe is just visible on the plate published in Shara et al. (1985) (their Fig. 8). Comparison shows that this tip has moved by roughly 2.5 arcsec in the intervening 20 years. Within the uncertainties, this proper motion is consistent with a 1670 ejection event.

**Table 3.** Line fluxes for the different knots, as measured from the INT image. For knot 3, the flux includes a non-subtracted star. The values for knots 6 and 7 are also uncertain. The uncertainty in the flux conversion factor is estimated at 10 per cent. The [N II] 6584/H $\alpha$  ratios are indicative only.

Knot	Flux [ $10^{-15}$ erg cm $^{-2}$ s $^{-1}$ ]	$v_{\text{hel}}$ [km s $^{-1}$ ]	[N II]/H $\alpha$
1	43		
2	28	-80	1.5
3	$\leq 25$	+0	1
4	4.7	+60	> 10
5	3.6		
6	1.7		
7	2.6		
southern tip		-175	> 2

### 3.3.1 Brightness

We measured fluxes for the different knots as follows: The  $r'$  magnitudes of 12 field stars were obtained from the IPHAS catalogues. The magnitudes were converted to Bessell filters on Landolt standard stars using the colour transformations

$$r' - R_{\text{Lan}} = +0.275(R - I)_{\text{Lan}} + 0.008$$

$$(r' - i') = 1.052(R - I)_{\text{Lan}} + 0.004$$

The magnitudes were converted into flux units per  $\text{\AA}$  using the Bessell et al. (1987) coefficients for R. The integrated in-band flux was obtained by multiplying by the equivalent width of the filter (80 $\text{\AA}$ ); this was divided by the data count (ADU) for each star to get a flux per data count. We find a conversion value of  $(94 \pm 6) \times 10^{-20}$  erg cm $^{-2}$  s $^{-1}$  per data count. This factor was applied to the data counts for each of the knots in the continuum-subtracted image.

The results are listed in Table 3. The line fluxes contain contributions from H $\alpha$ , and from the two [N II] lines: the filter transmission is within 5% of the peak transmission for each of the lines. Based on the spectroscopic data, H $\alpha$  accounts for typically half to a quarter of the measured line flux, but for knot 4 we do not detect H $\alpha$ .

The changes between the two INT images, measured in the same way, indicate a 0.08 mag (approx. 10%) change in the brightness of the knots, but this varies between knots by more than 10%. The standard deviation for the background stars alone is 0.05 mag, so that we do not see conclusive evidence for brightness evolution.

The brightest knots are those closest to the radio source. This suggest that their excitation arises from a central source.

### 3.4 Spectroscopy

Our echelle spectra show [N II] 6584/H $\alpha$  ratios between 1 and 5. Individual values are listed in Table 3. Because of the low S/N, these need confirmation. Knot 4 has no H $\alpha$  detected and could have a very high ratio.

These ratios can be compared to other values reported in the literature. Shara et al. (1985) analyze spectra of the three brightest nebulosities, numbered 1–3. They find consistent line intensities, with remarkably strong [S II] emission

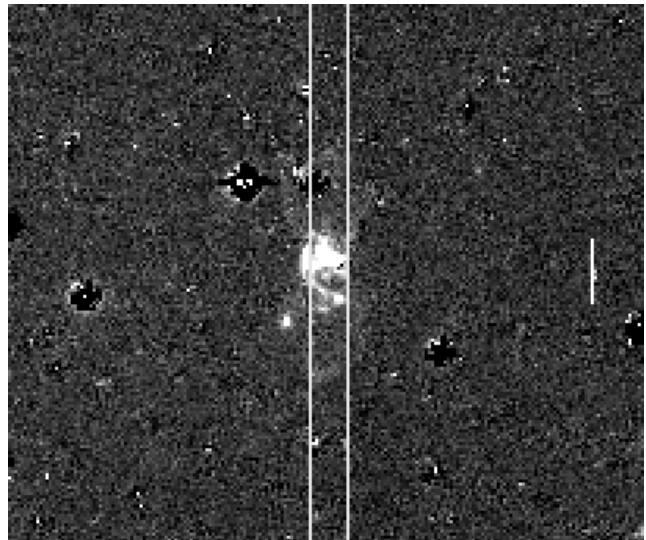


**Figure 7.** Positions of the two long slit echelle spectra discussed in the text. The scale bar is 20 arcsec long.

comparable to H $\alpha$ , and a ratio [N II]6584/H $\alpha \approx 3$ . The [S II] 6716/6730 line ratio is approximately two. [O III] is also seen, several times brighter than H $\beta$ , but weakened by the extinction.

A spectrum of a faint knot is reported by Naylor et al. (1992). The knot has [N II] 6584/H $\alpha \approx 1$ , and a [S II] 6716/6730 ratio of unity. It is not clear which knot this represents: their slit orientation at position angle 45 degrees covered knot 4 and 6. Our much higher line ratio for knot 4 suggests Naylor et al. observed knot 6.

A spectrum taken with a 4-arcsec slit oriented perpendicular to this direction is reported by Cohen (1985). Their spectrum shows intermediate values for both the N and S line ratios compared to the previous two papers.

### 3.5 Kinematics

The two long-slit spectra with better signal to noise are shown in Fig. 8; only signal from the relatively bright knots in the core was recorded. The top and middle panels in Fig. 8 show both the H $\alpha$  and [N II] 6584 $\text{\AA}$  emission lines for each slit position. The locations of the slits are shown in Fig. 7. The first slit (top panel) intersects knot 2 and a section of the southern arc, whereas the second slit (middle panel) located to the West of the previous one, intersects knot 3 and the edge of knot 4. The lower panel shows the corresponding P–V arrays for the [N II] 6584 $\text{\AA}$  line with heliocentric velocity scales.

The spectra show that the [N II] 6584 $\text{\AA}$  line is consistently stronger than H $\alpha$ . Although H $\alpha$  is barely detected, the S/N is enough to show that its line profile follows the same wide structure of [N II] 6584 $\text{\AA}$ . The line profiles are peculiar in the sense that the emission seems to arise only from localised regions and with a wide velocity range, of the order of 350 km s $^{-1}$ , somehow akin to those observed in supernovae blasts (e.g. Riego & López 2005).

The brightest region of each line profile yields the following heliocentric velocities: for knot 2 we find an approximate velocity of -80 km s $^{-1}$ ; for knot 3, 0 km s $^{-1}$ ; for

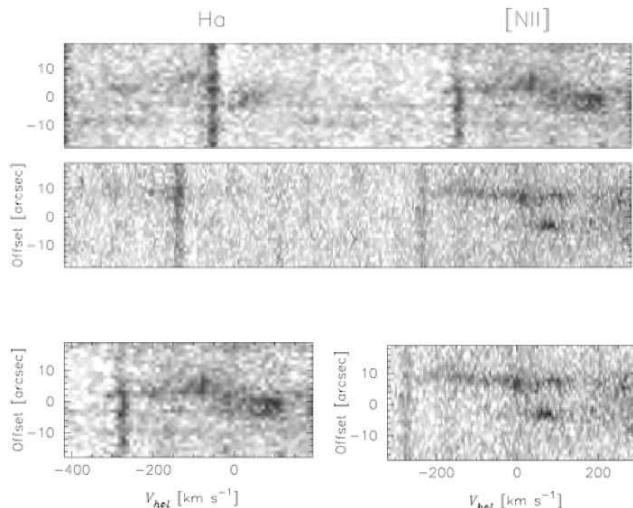


**Figure 8.** Two long slit echelle spectra. The upper frames show the full order, covering H $\alpha$  and [N II] 6584Å. The two lower frames show only the [N II] line. Lower left frame: knot 2 (upper) and the southern arc (lower emission). Lower right frame: knot 3 (upper) and knot 4 (lower emission).

knot 4,  $+60 \text{ km s}^{-1}$  and for the southern arc,  $+70 \text{ km s}^{-1}$ . From these line profiles the systemic velocity cannot be determined with confidence. However, since the observed heliocentric velocities are heavily blue-shifted for knots 2 & 3, it is reasonable to assume that there we are detecting material that is mainly coming towards us whereas the opposite is observed in knot 4 and the southern arc. From this kinematic behaviour and the morphology of the region (see Fig. 3) a possible interpretation is that of a rapidly expanding (and disrupted) torus or equatorial structure, centred at roughly  $-50 \text{ km s}^{-1}$  and where knots 2 & 3 are part of the foreground (approaching) equatorial structure and knot 4 and the southern arc are part of the background (receding) part of the torus.

The tip of the southern lobe was covered by two of the slit settings. There is a faint trace in both spectra of a velocity feature at the location of the tip with a velocity of about  $-175 \text{ km s}^{-1}$ . The sign and magnitude of this velocity is consistent with the bipolar lobes being oriented perpendicular to the equatorial structure discussed above and with the northern lobe moving away and the southern one coming towards us.

The kinematics and structure of the line profiles discussed here indicate that shocks are a main, if not the only, contributor to the excitation of these emission lines, in agreement with the arguments of the preceding section.

## 4 PHYSICAL PARAMETERS

### 4.1 Extinction distance

The spectra of Shara et al. (1985) show a strong Balmer decrement, corresponding to  $E(B - V) = 0.82 \pm 0.23$ , or  $A(V) = 2.5$ . Based on the weighted mean of this and the extinction towards a distant field star ( $E(B - V) = 0.7 \pm 0.1$ ), they adopt  $A(V) = 2.2 \pm 0.3$ .

Shara et al. (1985) locate the nebula beyond an extinction layer, located at  $550 \pm 150 \text{ pc}$  distance. Weight et al. (1993) deduce an upper limit of 2 kpc: they detect two CO clumps, with kinematic distances of 500 pc and 2 kpc. The two clumps together would result in  $E(B - V) = 1.25$ , suggesting that CK Vul must lie in front of the more distant clump.

We have assessed the IPHAS photometry of point sources in the vicinity of CK Vul to constrain the distance-extinction relation in this field. Within a field of  $4.5' \times 4.5'$ , we find a few essentially unreddened main sequence stars, and then a dearth of stars to  $A_V \sim 1.2$  ( $E(B - V) \simeq 0.4$ ). This jump in extinction may represent the dust layer at 550 pc described by Shara et al. (1985). We have cross-identified a group of 10 early A stars (presumed to be dwarfs) for which there are 2MASS *JHK* measurements as well as IPHAS *r'*, *i'* and H $\alpha$  data, and used them to obtain a sample of reddenings and distances consistent with their likely spectral types. These early A stars range in brightness between  $r' \sim 14$  and  $r' \sim 18$ , and are consistent with extinctions in the range  $0.9 \pm 0.2 < A_V < 5.4 \pm 0.5$ . The deduced distances fall in the range 2–4 kpc. The reddening does not increase in any organised manner with distance, and the extinction layer(s) appear to be patchy.

We will here use a distance of 600 pc. The extinctions indicate an upper limit for the distance of CK Vul of 4 kpc.

### 4.2 Velocities

The radial velocity range is about  $350 \text{ km s}^{-1}$ . The highest blue-shifted velocities are seen just to the north of knot 2 and may represent the inner edge of the bipolar lobe, oriented close to the line of sight along the edge of the torus. We do not see a similar extended velocity structure at red-shifted velocities. This may be due to the placement of the slits, or may indicate some internal extinction at that location. The southern tip is blue-shifted at  $-175 \text{ km s}^{-1}$ : similar to the extreme velocity near the torus, but likely less inclined towards us.

The proper motion of the knots 4 and 5 are around  $37 \text{ mas/year}$  and  $59 \text{ mas/year}$  respectively. For the outer tips of the bipolar lobes, the radial distance to the central radio source of 35 arcsec indicates a proper motion of  $105 \text{ mas/year}$ . Our measured proper motion of the southern tip corresponds to  $120 \pm 25 \text{ mas yr}^{-1}$ . For a distance of 600 pc, the respective tangential velocities are 106 and 169 km/s for the knots, and  $340 \text{ km s}^{-1}$  for the tips of the bipolar lobes. Assuming a systemic velocity  $v_{\text{hel}} = -50 \text{ km s}^{-1}$ , the space velocity of the tip of the bipolar lobe becomes  $v_{\text{ej}} \approx 360 \text{ km s}^{-1}$ .

The bipolar flow is inclined by 20 degrees with respect to the plane of the sky, from these numbers.

### 4.3 Extended nebula

The nebula is detected only in ionized lines and in dust. It is possible that emission lines reveal only part of the nebula, with the remainder not ionized or too faint. Parameters of the extended nebula must therefore depend on estimations.

Shara et al. (1985) derive  $n_e < 10^2 \text{ cm}^{-3}$ , based on the [S II] line ratio in knot 1. Naylor et al. (1992) find a higher

density  $n_e \approx 10^3 \text{ cm}^{-3}$ , based on the [S II] line ratio of a faint knot (possibly knot 4 or knot 6). If we assume that the system of knots 1,2,3,4,6 represents a partially ionized torus with density  $n = 10^2 \text{ cm}^{-3}$ , diameter of 10 arcsec, thickness and height of 5 arcsec, the total mass becomes  $M \sim 2 \times 10^{-5} M_\odot$ . If, on the other hand, we assume that the total extent is given by the bipolar nebula (35 arcsec radius), and assume a typical density of  $n = 10^2 \text{ cm}^{-3}$ , the total mass becomes  $M \sim 2 \times 10^{-2} M_\odot$ . The dust mass derived by Evans et al. (2002) gives  $M \sim 5 \times 10^{-2} M_\odot$  for a typical dust-to-gas ratio of 100 (assuming hydrogen-rich gas). Thus, a model of a cloud of radius 30 arcsec and average density  $n = 10^2 \text{ cm}^{-3}$  is consistent with observational constraints.

Shara et al. (1985) suggests that the extended nebula was ionized during the 1670 eruption and is now recombining. This assumption of a slowly recombining nebula presents some problems.  $\text{N}^+$  recombines much faster than hydrogen, so the high [N II]/ $\text{H}\alpha$  ratio would require that no significant recombination has yet occurred even in the denser knots. For [N II], at a density of  $100 \text{ cm}^{-3}$  the recombination time scale is 75 yr (Lechner & Kimeswenger 2004). Densities of  $n_e \gtrsim 10^2 \text{ cm}^{-3}$  require continuous ionization.

The line ratios listed by Shara et al. (1985) are in good qualitative agreement with the radiative shock models of McKee & Hollenbach (1980), although  $\text{H}\alpha$  is somewhat fainter than seen in those models. In particular, the [S II]  $6716+6730/\text{H}\alpha \sim 1$ , [N I]  $5200/\text{H}\beta \sim 1$  and the strength of the [N II]  $6584\text{\AA}$  line are indicative of shock velocities  $v \sim 100 \text{ km s}^{-1}$ . (Shara et al. (1985) do not list or identify the [N I]  $5200\text{\AA}$  line, but it is apparent in their spectrum.) The presence of [O III], if shock-ionized, indicates shock velocities above  $100 \text{ km s}^{-1}$ .

## 5 THE COMPACT RADIO SOURCE

### 5.1 Emission mechanism

The fact that we have a compact but resolved source suggests thermal free-free emission for the origin of the radio emission. This is supported by the observed brightness temperature. At 5 GHz, the observed diameter (0.11 arcsec FWHM of a deconvolved gaussian) gives a brightness temperature of  $T_b = 6000 \text{ K}$ . At 8 GHz we find  $T_b = 2000 \text{ K}$ . Assuming the electron temperature is  $T_e = 10^4 \text{ K}$ , the optical depth at 5 GHz is  $\tau \approx 0.9$ . This predicts at 8 GHz that  $T_b \approx 2700 \text{ K}$ , in reasonable agreement with observations. The emission is optically thick at 1.4 GHz, explaining the non-detection at this frequency (Bode et al. 1987).

The lack of an infrared counterpart presents a problem, however. Optically thin free-free emission predicts approximately 0.6 mJy at  $8\mu\text{m}$ , assuming a  $\nu^{-0.1}$  index. The upper limit for a counterpart to the radio source at  $8\mu\text{m}$  is around 0.2 mJy. The only possible non-stellar source is a possible faint source 2 arcsec south-east of the radio source, which is absent from the Spitzer images at shorter wavelengths. The lack of an  $8\mu\text{m}$  detection can be explained by very high extinction. However, it also suggests to explore different emission mechanism.

Small grains can emit appreciable radio emission through their rotation. The electric dipole emission is described in Draine & Lazarian (1998) and references

therein. Using emissivities per hydrogen atom tabulated in Draine & Lazarian (1998), we find that our radio flux would require  $\sim 3 \times 10^{-3} M_\odot$  of gas (assuming normal composition of the gas). This is a plausible value for the radio source, and would give densities around  $n \sim 10^7 \text{ cm}^{-3}$ . However, this emission produces a positive spectral index between 5 and 8 GHz, while we find a flat flux distribution. There is also no evidence for the required very small grains in the infrared spectral energy distribution.

Synchrotron and cyclotron emission (Linksy 1996), from relativistic electrons moving in a magnetic field, give brightness temperatures much higher than we observe. However, if our radio source is found not to be resolved, this becomes a possibility.

### 5.2 Density and mass of the radio core

If the radio emission is due to free-free emission, we can derive some parameters of the originating nebula. Using the observed flux and assuming  $\tau = 0.9$  and  $T_e = 10^4 \text{ K}$  at 5 GHz, the emission measure becomes  $\text{EM} = n_e^2 l = 8.1 \times 10^7 \text{ pc cm}^{-6}$  where  $n_e$  is the electron density and  $l$  the depth of the emitting region. The latter is taken as the same as the FWHM of the radio source (assuming symmetry), or 66 AU at 600 pc.

We arrive at a density of  $N_e = 5 \times 10^5 \text{ cm}^{-3}$ . The mass of the ionized region becomes  $M_i \approx 4 \times 10^{-7} M_\odot$ . This assumes a H-rich chemical composition: H-poor gas requires more mass per electron.

For a filling factor equal to unity, a relation between the hydrogen line flux and the optically thin free-free  $S_{5\text{GHz}}$  flux density is given by Pottasch (1984) assuming hydrogen-rich material. This gives an expected  $F_0(\text{H}\alpha) \approx 1.5 \times 10^{-12} \text{ erg s}^{-1} \text{ cm}^{-2}$ . The IPHAS  $\text{H}\alpha$  filter has an equivalent width of approximately  $80\text{\AA}$  and a peak transmission of 90 per cent (Drew et al. 2005): the unreddened magnitude of the central object in the  $\text{H}\alpha$  filter should have been  $m \sim 12.3$ . The (undetected) object is much weaker. The emission located 0.5 arcsec away from the radio source is  $1.6 \times 10^{-15} \text{ erg s}^{-1} \text{ cm}^{-2}$ , three orders fainter. This requires  $A_R \geq 7.5$ , corresponding to  $A_V \geq 10$  for a standard extinction law and pure  $\text{H}\alpha$  emission.

The [N II]  $6584/6548\text{\AA}$  lines are within the IPHAS  $\text{H}\alpha$  filter transmission. However, these lines have a critical density of  $n_{\text{cr}} = 9 \times 10^4 \text{ cm}^{-3}$ . We derive an electron density of  $n_e = 5 \times 10^5 \text{ cm}^{-3}$ , suggesting that these lines do not contribute in the central region.

The lack of a clear  $\text{H}\alpha$  counterpart to the radio source can also be interpreted as evidence that the core is H-poor. Hydrogen-poor gas tends to have lower electron temperatures, as the cooling per nucleus is more efficient. We ran some *Cloudy* models to obtain indicative values. The models are similar to those described in Hajduk et al. (2005), but use a PG1159 stellar model (Rauch 2003), with luminosity  $L = 0.5 L_\odot$ , a density  $n_e = 5-7 \times 10^5 \text{ cm}^{-3}$  (depending on stellar temperature  $T_{\text{eff}}$ ) and an inner radius of 13 AU. For  $T_{\text{eff}} = 60, 80, 100, 120 \text{ kK}$ , we find  $T_e = 8100, 8400, 8700, 9200\text{K}$ , respectively. These are lower than corresponding values of H-rich gas, but not dramatically so. The physical cause of the relatively high temperatures is the suppression of the forbidden lines at these high densities, which reduces the cooling rate. The model temperatures are within the

range derived from the radio free-free spectrum. But in the absence of measured line ratios, the models are exploratory only.

### 5.3 Luminosity

The recombination timescale of the radio core is less than a year. The central region is therefore continuously ionized: although no central star is visible, its continuing existence can be inferred. Recombining gas can also be ruled out because it would show a very low electron temperature  $T_e \sim 10^3$  K, much lower than the observed brightness temperature.

The luminosity of the ionizing star can be estimated assuming that all photons above the Lyman limit ionize hydrogen, and that the object emits as a black body. The number of ionizing photons reaches a maximum at a temperature of about  $T_* = 7 \times 10^4$  K. For this temperature, the required black body luminosity is  $L_* = 0.5 L_\odot$ . For other temperatures within the range 40–100 kK, the luminosity is within a factor of 1.5 of this value. Stellar atmosphere models require a little higher luminosity as a black body emits more ionizing photons than a realistic atmosphere of the same temperature (e.g., at  $T = 50$  kK, a Kurucz model gives 10 % fewer H-ionizing photons than does a black body). Geometrical considerations also indicate that this luminosity is a lower limit, and the real luminosity could be a few times higher.

Such a luminosity, combined with a high stellar temperature, gives an unreddened magnitude of order  $V_0 \gtrsim 17$ . No star is detected near this magnitude. The ROSAT all sky survey did not detect any source at the position of CK Vul. Sevelli (2004) reports extreme faintness of CK Vul in the SWP IUE spectra; the aperture of the instrument included the position of the radio source. The lack of detection may be due to a higher stellar temperature together with high obscuration.

For comparison, at the adopted distance, the peak absolute magnitude of the AD1670 eruption was around  $M(V)_0 \approx -9$  to  $-8$ . The current luminosity implied by the radio source is a factor of  $10^5$  fainter.

### 5.4 Dust

The infrared spectrum of CK Vul (Evans et al. 2002) shows two components, with dust temperatures around 550 K and 25 K. Their two-component dust model yields approximate dust masses of  $1.5 \times 10^{-9}$  and  $5 \times 10^{-4} M_\odot$ . The mass of the first component agrees well with the derived ionized mass, assuming normal dust-to-gas ratios. The model was based on IRAS flux densities: the large IRAS apertures include both the core and the extended nebula, and the second component may be identified with the extended nebula.

The new high-resolution Glimpse limit is a factor of 100 below the IRAS  $12\mu\text{m}$  flux. We ran dust models with parameters  $r_i = 2 \times 10^{14}$  cm,  $r_o = 10^{15}$  cm, density at inner edge  $5 \times 10^5 \text{ cm}^{-3}$ , density distribution  $n \propto r^{-1}$ , and a star with  $T = 6 \times 10^4$  K and  $L = 0.5 L_\odot$ . The (assumed H-rich) shell has a mass consistent with the ionized mass. For silicate dust, this yields predicted flux densities of  $F_8 = 0.1$  mJy and  $F_{12} = 0.6$  mJy, well within observational limits. Carbon-rich dust (as assumed by Evans et al. (2002) for their hotter dust

component) would be several times brighter at  $8\mu\text{m}$ . These exploratory models differ from Evans et al. (2002) mainly in that they give lower dust temperatures (200–300 K).

The peculiar light curve with several dips may be due to epochs of dust formation. In support of this, Hevelius comments that during the second peak (April 1671), the source appeared reddish (Shara et al. 1985). The brightness of the initial eruption suggest that it did not suffer the line-of-sight extinction of the current radio source, and that the dust formed afterwards.

## 6 THE NATURE OF CK VUL

### 6.1 Observational constraints

The current luminosity and high temperature places the central object high on the white dwarf cooling track, e.g., a  $1 L_\odot$  white dwarf has  $T_{\text{eff}} \approx 65$  kK and a cooling age of  $t_c \sim 10^6$  yr (Bloeker 1995).

The compactness of the radio source implies it is not expanding, as the expansion velocity would be less than  $1 \text{ km s}^{-1}$ , or below the escape velocity. We can therefore assume that the radio nebula is part of a stable structure, such as a rotating disk, and could predate the eruption. The bipolar lobes are similar to those found in some young planetary nebulae and post-AGB stars. Such lobes can form where a spherical fast wind meets an existing equatorial obstruction (Icke 1987).

An area of low dust emission surrounding CK Vul is seen in IRAS images (Evans et al. 2002). This resembles cases where the ISM has been swept up by a stellar wind (Zijlstra & Weinberger 2002) and suggests CK Vul has gone through phases of high mass loss over the past  $\sim 10^5$ – $10^6$  yr.

Together, these constraints favour an evolved object, and the morphology favours a binary object. Two possible interpretations are a nova, and a thermal pulse.

One should consider whether a supernova classification can truly be ruled out. The  $[\text{S II}]/\text{H}\alpha \sim 1$  ratio is diagnostic of supernova remnants. Also, the current luminosity is a typical value for a pulsar, and the radio spectrum is similar to pulsar wind nebulae (e.g. Temim et al. 2006). The object H 2-12, a knot inside the Kepler supernova remnant, shows similar line ratios and velocities to CK Vul (Riesgo & López 2005). However, there is no X-ray source at this position, nor is there significant radio emission from the extended nebula. The bipolar symmetry of CK Vul differs from the structures seen in supernova remnants. We conclude that a supernova classification is unlikely.

A ‘gentle’ supernova (Tout 2006) can be considered. An accreting helium white dwarf may ignite its helium at masses far below the Chandrasekhar mass (Woosley & Weaver 1994). The lack of observational evidence for sub-luminous supernovae suggests that the ignition under such conditions may be non-explosive. However, such objects may also have been classified wrongly. The models of Woosley & Weaver (1994) predict short-lived maxima, however.

The observations do not clearly support the possibility of a stellar merger (Kato 2003): a merger would be able to explain the large drop in luminosity since the eruption, but would lead to a bloated, cool star. The radio source requires an ionizing star.

## 6.2 A light nova

Classical novae are dominated by massive white dwarfs: these show frequent eruptions, but consequently eject relatively little mass. A lower-mass white dwarf with a low accretion rate can eject the most massive shell. However, such eruptions are rare as a consequence of the much longer accretion time scales. The current luminosity of CK Vul corresponds to an accretion rate of  $\dot{M}_{\text{acc}} \sim 10^{-10} M_{\odot} \text{ yr}^{-1}$ . The peak temperature, for a thermal-nuclear runaway on a low-mass white dwarf, may not even reach  $10^8 \text{ K}$  limiting the nucleosynthesis which occurs (Starrfield 2007).

A large set of models covering a range of parameter space is presented by Prialnik & Kovetz (1995). Some of these approach the constraints set by CK Vul. For instance, their model with  $M_{\text{WD}} = 0.65 M_{\odot}$ ,  $T_{\text{WD}} = 3 \times 10^7 \text{ K}$  and  $\dot{M} = 10^{-10} M_{\odot} \text{ yr}^{-1}$  yields an ejection velocity of  $200 \text{ km s}^{-1}$ , eruption amplitude of 16 mag, mass-loss time scale of 480 days (during which time the nova remains bright), and a very high peak luminosity of  $L = 8 \times 10^4 L_{\odot}$  ( $M_{\text{bol}} = -7.5$ ). The recurrence time scale of this model is  $10^6 \text{ yr}$ .

This particular model gives an ejecta mass of  $10^{-4} M_{\odot}$ . The highest predicted ejecta mass for a light nova is only  $7 \times 10^{-4} M_{\odot}$  (Yaron et al. 2005). On the one hand, this is three orders of magnitude higher than found in near-Chandrasekhar-mass novae. On the other hand, it is one to two orders of magnitude below the derived nebular mass of CK Vul (and below the mass in the dust alone). It is however possible that part of this is swept-up material which predates the eruption.

## 6.3 A thermal pulse

Helium ignition on the white dwarf cooling track has been observed in V605 Aql (Clayton et al. 2006) and V4334 Sgr (Sakurai's Object: Asplund et al. 1999; Hajduk et al. 2005; Evans et al. 2006). Their light curves show similarities to CK Vul: a long lived maximum at  $M \sim -5$ , with a brief phase of very high, dusty mass loss. Three further objects are known to have experienced a VLTP event in their evolution, as shown by the presence of hydrogen-poor central regions within a planetary nebula (Zijlstra 2002). Outflow Velocities are also similar, with observed values are  $\sim 250 \text{ km s}^{-1}$  for V605 Aql (Pollacco et al. 1992) and V4334 Sgr (Kerber et al. 2002).

If CK Vul is a VLTP, it would fall on an evolutionary sequence V4334 Sgr (Sakurai's Object: 10 yr), V605 Aql (90 yr), IRAS 15154–5258 ( $\sim 10^3 \text{ yr}$ ) and the two more evolved objects A30/A78 (Zijlstra 2002). The first two are still hidden inside a dense cocoon of dusty ejecta, but like CK Vul the central object is seen in radio emission. There are some morphological resemblances with CK Vul, with the ejecta in these objects showing equatorial torii and polar knots. The origin of the morphologies are not known.

There are however also notable differences. The radio source in CK Vul is much more compact than expected: in V605 Aql, which is at a larger distance, the 0.3-arcsec dense shell is expanding and there is no evidence for a non-expanding component. The ejecta in both VLTP objects are almost completely H-poor. In contrast, most knots in CK Vul show significant H $\alpha$  components, even if fainter than

expected. (We do not detect H $\alpha$  emission in knot 4, which is likely H-poor. It is possible that the other knots have swept up ambient hydrogen.) CK Vul has a much lower current luminosity than the other five objects. Finally, fossil planetary nebulae are seen in all five objects, but CK Vul only shows a surrounding hole in the ISM as evidence for past mass loss: this suggests a much longer post-AGB time scale before its eruption.

VLTP events may show a characteristic double loop in the HR diagram, over a time scale of a few hundred years (Hajduk et al. 2005). Direct observational evidence for a second loop is still lacking and the VLTP scenario is not well understood (Miller Bertolami et al. 2006). Observations during the 18<sup>th</sup> and 19<sup>th</sup> century (Shara et al. 1985) provide no indications for a second, decadal phase of high luminosity and low temperatures for CK Vul, as predicted by double-loop models, but the extinction may have hidden such an event. However, the low luminosity we derive is a severe constraint for such models.

### 6.3.1 Accretion-induced pulse

The morphology shows similarities to evolved binary systems, such as symbiotics. This together with the compact radio source suggests variation on the standard VLTP scenario can be considered, involving accretion.

A group of binary post-AGB stars, including RV Tau stars, show compact circumstellar disks, with typical sizes of 10-100 AU (van Winckel 2003; de Ruyter et al. 2006). The disks form when a close binary ( $P \sim 1 \text{ yr}$ ) captures matter lost by the central star into a circumbinary disk. The radio source in CK Vul has the correct size to be the remnant of such a disk. CK Vul shows similarities in particular with OH231.8+4.2, which shows bipolar lobes, an inner disk with diameter of 50 AU as well as a 1000 AU dense torus (Matsuura 2006).

In such a system, the post-AGB evolution may be affected by accretion from the disk on the post-AGB star (Zijlstra et al. 2001). Such accretion could trigger a thermal pulse later during the post-AGB evolution than would otherwise occur. The circumstellar environment can explain the bipolar outflows. This possibility should be explored further for CK Vul.

## 7 CONCLUSIONS

A compact radio source allows us for the first time to identify the central object of the old nova CK Vul. The radio emission is modelled as thermal free-free emission, from a compact nebula of diameter  $\sim 60 \text{ AU}$ . The density of the nebula is  $n_e = 5 \times 10^5 \text{ cm}^{-3}$ . A high extinction through the circumstellar shell is indicated by the lack of H $\alpha$  detection at the position of the radio source. The ionization requires a luminosity of the ionizing object of order  $1 L_{\odot}$ .

Deep H $\alpha$  images reveal a large bipolar outflow, with a diameter of 70 arcsec. The nebulosity is brightest near the position of the radio source, and shows various components. Comparison with previous images shows significant expansion of the nebula. Extrapolating back shows that the H $\alpha$  structures were ejected in the AD 1670 eruption. The centre

of expansion is, within the uncertainties, identical to the radio source. Echelle spectra and proper motions give original ejecta velocities of  $\sim 360 \text{ km s}^{-1}$ .

The observed characteristics differ from classical novae. New models of nova eruption on cool, low-mass white dwarfs can explain some of the observational constraints. A classification as a Very Late Thermal Pulse appears possible, possibly accretion-induced. The radio source is proposed to be the remnant of a circumbinary disk, as seen in some binary post-AGB stars. The ejecta morphology are suggestive of binary interaction. The radio source provides important information on the environment of CK Vul. However, at present CK Vul still remains an enigma (Evans et al. 2002; Naylor et al. 1992; Shara et al. 1985).

## ACKNOWLEDGMENTS

We thank Antonio Garcia, Kerttu Viironen and Ramarao Tata for carrying out the INT observations. The VLA is part of the National Radio Astronomy Observatory, operated by AUI inc on behalf of the NSF. The INT is part of the ING group of telescopes. This project was supported by a NATO grant for collaborative research, by PPARC through a rolling grant, and by Uniwersytet Mikolaja Kopernika through grant UMK 366-A. PvH acknowledges support from the Belgian Science Policy Office through grant MO/33/017. JAL and MGR acknowledge financial support from CONA-CyT grant 43121 and UNAM-DGAPA grants IN108506-2, IN108406-2, and IN112103. AAZ thanks the SAAO for hospitality during a sabbatical visit.

## REFERENCES

- Asplund M., Lambert D.L., Kipper T., Pollacco D., Shetrone M.D., 1999, *A&A*, 343, 507  
 Bessell M.S., Castelli F., Plez B., 1998, *A&A*, 333, 231  
 Bode M.F., Seaquist E.R., Evans A., 1987, *MNRAS*, 228, 217  
 Bloeker T., 1995, *A&A*, 299, 755  
 Clayton G.C., Kerber F., Pirzkal N., De Marco O., Crowther P.A., Fedrow J.M., 2006, *ApJ*, 646, L69  
 Cohen J.G., 1985, *ApJ*, 292, 90  
 de Ruyter S., van Winckel H., Maas T., Lloyd Evans T., Waters L. B. F. M., Dejonghe H., 2006, *A&A*, 448, 641  
 Draine B.T., Lazarian A., 1998, *ApJ*, 508, 157  
 Draine B.T., Lazarian A., 1999, *ApJ*, 512, 740  
 Drew J.E., Greimel R., Irwin M.J., Aungwerojwit A., Barlow M.J., Corradi R.L.M., Drake J.J., et al., 2005, *MNRAS*, 362, 753  
 Evans A., Tyne, V.H., van Loon J.Th., Smalley B., Geballe T.R., Gehrz R.D., Woodward C.E., Zijlstra A.A., Polomski E., Rushton M.T., Eyres, S.P.S., Starrfield S.G., Krautter J., Wagner R.M., 2006, *MNRAS*, 373, L75  
 Evans A., van Loon J.Th., Zijlstra A.A., Pollacco D.L., Smalley, B., Tyne, V.H., Eyres, S.P.S., 2002, *MNRAS*, 332, 35  
 Hajduk M., Zijlstra A.A., Herwig F., van Hoof P.A.M., Kerber F., Kimeswenger S., Pollacco D.L., Evans A., Lopèz J.A., Bryce M., Eyres S.P.S., Matsuura M., 2005, *Science*, 308, 231  
 Harrison T.E., 1996, *PASP*, 108, 1112  
 Icke V., 1989, *A&A*, 211, 409  
 Kato T., 2003, *A&A*, 399, 695  
 Kerber F., Pirzkal N., De Marco O., Asplund M., Clayton G.C., Rosa M.R., 2002, *ApJ*, 581, L39  
 Lechner M.F.M., Kimeswenger S., 2004, *A&A*, 426, 145  
 Linksy J.L., 1996, in: *Radio emission from the stars and the Sun*, A.R. Taylor, J.M. Paredes (Eds.), *ASP Conf. Ser.*, 93, 439  
 Matsuura M., Chesneau O., Zijlstra A.A., Waters L. B. F. M., Jaffe W., Yates J., Gledhill T., 2006, *ApJ*, 646, L123  
 McKee C.F., Hollenbach D.J., 1980, *ARA&A*, 18,219  
 Meaburn J., López J.A., Gutiérrez L., Quiróz F., Murillo J.M., Valdéz J., Pedrayez M., 2003, *RMxAA*, 39, 185  
 Miller Bertolami M.M., Althaus L.G., Serenelli A.M., Panei J.A., 2006, *A&A*, 449, 313  
 Naylor T., Charles P.A., Mukai K., Evans A., 1992, *MNRAS*, 258, 449  
 Pollacco D.L., Lawson W.A., Clegg R.E.S., Hill P. W. 1992, *MNRAS* 257, 33P  
 Pottasch S.R., 1984, *Planetary Nebulae, a Study of Late Stages of Stellar Evolution* (Dordrecht: Reidel)  
 Prialnik D., Kovetz A., 1995, *ApJ*, 445, 789  
 Rauch T., 2003, *A&A*, 403, 709  
 Riesgo H., López J.A., 2005, *RMxAA*, 41, 57  
 Ruffle P., Zijlstra A.A., Walsh J.R., Gray M.D., Gesicki K., Minniti D., Comeron F., 2004, *MNRAS*, 353, 796  
 Seaquist E.R., Bode M. F., Frail D.A., Roberts J.A., Evans A., Albinson J.S., 1989, *ApJ*, 344, 805  
 Sevelli P., 2004, *BaltA*, 13, 93  
 Shara M.M., Moffat A.A., 1982, *ApJ*, 258, 41  
 Shara M.M., Moffat A.A., Webbink R.F., 1985, *ApJ*, 294, 271  
 Starrfield S., 2007, in: *Classical Novae*, 2<sup>nd</sup> ed., M. Bode & A. Evans (eds.), in press  
 Temim T., Gehrz R.D., Woodward C.E., Roellig Th.L., Smith N., Rudnick L., Polomski E.F., Davidson K., Yuen L., Onaka T., 2006, *AJ*, 132, 1610  
 Tout C.A., 2006, *MmSAI*, 77, 804  
 van Winckel H., 2003, *ARA&A*, 41, 391  
 Warner B., 2006, *Astronomy & Geophysics*, 47, 29  
 Weight A., Evans A., Albinson J.S., Krautter J., 1993, *A&A*, 268, 294  
 Woosley S.E., Weaver T.A., 1994, *ApJ*, 423, 371  
 Yaron O., Prialnik D., Shara M.M., Kovetz A., 2005, *ApJ*, 623, 398  
 Zacharias N., Urban S.E., Zacharias M.I., Wycoff G.L., Hall D.M., Monet D.G., Rafferty T.J., 2004, *AJ*, 127, 3043  
 Zijlstra A.A., 2002, *Ap&SS*, 279, 171  
 Zijlstra A.A., Weinberger R., 2002, *ApJ*, 572, 1006  
 Zijlstra A. A., Chapman J. M., te Lintel Hekkert P., Likkel L., Comeron F., Norris R. P., Molster F. J., Cohen R. J., 2001, *MNRAS*, 322, 280